Annals of Nuclear Energy 77 (2015) 415–424

Contents lists available at ScienceDirect

Annals of Nuclear Energy

journal homepage: www.elsevier.com/locate/anucene

CFD model of diabatic annular two-phase flow using the Eulerian–Lagrangian approach

Haipeng Li *, Henryk Anglart

Royal Institute of Technology (KTH), Stockholm 10691, Sweden

ARTICLE INFO

Article history:
Received 8 August 2014
Received in revised form 3 December 2014
Accepted 6 December 2014
Available online 17 December 2014

Keywords:
Annular two-phase flow
Liquid film flow
Lagrangian Particle Tracking
Droplet deposition and entrainment

ABSTRACT

A computational fluid dynamics (CFD) model of annular two-phase flow with evaporating liquid film has been developed based on the Eulerian–Lagrangian approach, with the objective to predict the dryout occurrence. Due to the fact that the liquid film is sufficiently thin in the diabatic annular flow and at the pre-dryout conditions, it is assumed that the flow in the wall normal direction can be neglected, and the spatial gradients of the dependent variables tangential to the wall are negligible compared to those in the wall normal direction. Subsequently the transport equations of mass, momentum and energy for liquid film are integrated in the wall normal direction to obtain two-dimensional equations, with all the liquid film properties depth-averaged. The liquid film model is coupled to the gas core flow, which currently is represented using the Eulerian–Lagrangian technique. The mass, momentum and energy transfers between the liquid film, gas, and entrained droplets have been taken into account.

The resultant unified model for annular flow has been applied to the steam–water flow with conditions typical for a Boiling Water Reactor (BWR). The simulation results for the liquid film flow rate show favorable agreement with the experimental data, with the potential to predict the dryout occurrence based on criteria of critical film thickness or critical film flow rate.

1. Introduction

Annular two-phase flow regime plays important role in many engineering applications such as heat exchangers and boiling channels. This type of flow regime can be encountered in a wide range of pressure, mass flow rates and flow qualities. In annular flow, the liquid phase flows partly as a thin liquid film on the channel wall and partly as entrained droplets in the gas core. In a diabatic annular flow, the liquid film is depleted by both the entrainment of liquid droplets and by evaporation. When the liquid film dries out and no longer covers the wall, the heat transfer coefficient significantly deteriorates, leading to the onset of boiling crisis called dryout. Prediction of the occurrence of dryout is crucial to the optimized design and operation of industrial systems such as, Boiling Water Reactors (BWRs). As a result, research has been continually focused on better understanding of the mechanisms that govern dryout and on the accurate numerical prediction of the dryout occurrence.

Due to the complexity of the governing phenomena, the dryout occurrence is still predominantly evaluated by employing empirical correlations, which are based on expensive experiments and apparently are limited to the specific range of geometries and operational conditions (Tong and Tang, 1997). The extrapolation of these correlations to systems and conditions much outside the range for which they were developed is of extremely doubtful validity. To resolve theses limitations, several phenomenological and mechanistic approaches for dryout prediction have been proposed.

On the one hand, the phenomenological modeling of annular flow was proposed to calculate the liquid film flow based on the rate of evaporation, and droplet deposition and entrainment (Hewitt and Govan, 1990; Okawa et al., 2003). In these types of approaches, the dryout is assumed to occur when the liquid film flow rate or corresponding film thickness decreases to zero or below a critical value (Zuber and Staub, 1966; Anglart, 2011, 2013). The phenomenological models are basically one-dimensional, with possible extensions to be coupled with a subchannel code. However, they heavily rely on the correlations for droplet deposition and entrainment (Kataoka et al., 2000; Adamsson and Le Corre, 2011).

On the other hand, mechanistic approaches employing the computational multi-phase fluid dynamics (CMFD) have been developed to simulate the annular flow (Lahey, 2005; Rodriguez, 2009). To accurately capture the detailed phenomena, e.g. the

* Corresponding author. Tel.: +46 0855378888; fax: +46 0855378216.
E-mail addresses: haipengl@kth.se (H. Li), henryk@kth.se (H. Anglart).

http://dx.doi.org/10.1016/j.anucene.2014.12.002
0306-4549/

gas–liquid interface in annular flow, however, CMFD is still expensive.

Damsohn (2011) provided an extensive literature study on the annular flow simulation, especially the liquid film modeling, among which a two-dimensional treatment is of concern. Bai and Gosman (1996) proposed a two-dimensional liquid film model, which can be coupled with the gas core flow into a unified framework for annular flow simulation (Adechy and Issa, 2004; Meredith et al., 2011). In these approaches the liquid film model includes mass, momentum and energy interactions (e.g. the droplet deposition and entrainment) with the gas core flow, which can be represented using Eulerian–Eulerian or Eulerian–Lagrangian techniques. The droplet behavior has been successfully investigated using the Lagrangian Particle Tracking (LPT) based on the Eulerian–Lagrangian simulation (Yamamoto and Okawa, 2010), with good capability to predict the droplet deposition (Caraghiaur and Anglart, 2013).

The liquid film entrainment is mainly due to the disturbance waves developed in the gas core–liquid film interface, however, it is difficult and expensive to quantitatively capture the behavior directly based on the disturbance wave simulation (Rodriguez, 2009). As a result, the inception and rate of entrainment is still dominantly predicted using the correlations developed based on entrainment mechanism, e.g. shearing off of a roll wave crest and undercutting of a liquid film (Ishii and Grolmes, 1975).

In the current work, the two-dimensional liquid film model is coupled to the gas core flow with the Eulerian–Lagrangian method to predict the liquid film thickness in diabatic upward annular flow with phase change.

2. Method

2.1. Liquid film modeling

In diabatic annular two-phase flow, e.g. a vertical pipe as shown in Fig. 1, the liquid phase flows partly as a thin liquid film on the heated wall and partly as droplets in the gas core. The liquid film, especially that in the upstream of the dryout point, is sufficiently thin to safely make the following major thin-film assumptions:

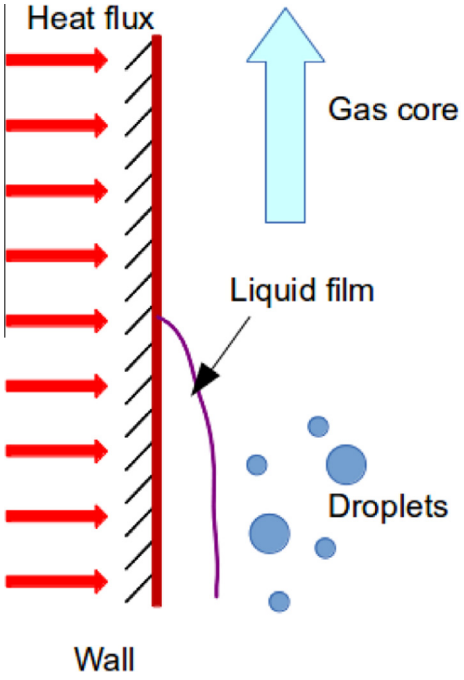

Fig. 1. Schematic of the diabatic upward annular flow with depleting liquid film.

- the flow in the wall normal direction can be reasonably assumed to be negligible,
- the spatial gradients of the dependent variables tangential to the wall surface are negligible compared to those in the wall normal direction.

These assumptions imply that the advection can be treated in the wall tangential direction and diffusion in the wall normal direction, as shown in Fig. 2. As a result, the transport equations for the liquid film can be integrated in the wall normal direction to obtain the two-dimensional equations. All the liquid film properties, which vary across the film thickness, appear as depth-averaged quantities and are in general defined as

$$\bar{\varphi} = \frac{1}{\delta}\int_0^{\delta} \varphi dz \tag{1}$$

where δ is the film thickness, φ is any liquid film property variable, and z is the coordinate for the wall normal direction. For simplicity, the bar is omitted for all the depth-averaged liquid film properties used in the following description. Then the mass, momentum, and energy equations are integrated in the wall normal direction as

$$\frac{\partial(\rho\delta)}{\partial t} + \nabla_s \cdot (\rho\delta\mathbf{U}) = S_\delta \tag{2}$$

$$\frac{\partial(\rho\delta\mathbf{U})}{\partial t} + \nabla_s \cdot (\rho\delta\mathbf{U}\mathbf{U}) = -\delta\nabla_s p + S_\mathbf{U} \tag{3}$$

$$\frac{\partial(\rho\delta h)}{\partial t} + \nabla_s \cdot (\rho\delta h\mathbf{U}) = S_h \tag{4}$$

where $\mathbf{U}$ is the mean film velocity, h is the mean film enthalpy, ∇_s is the nabla operator tangential to the surface, ρ is the density, p is the total pressure, and S_δ, $S_\mathbf{U}$ and S_h are the source terms. It is noted that the advection terms for all the equations are explicitly described, however, the diffusion and the external sources are modeled as source terms. The liquid film has complex interaction with the gas core flow, which means that corresponding models should be included as source terms to consider all the phenomena of concern.

2.1.1. Mass source terms

In diabatic annular flow, the mass sources and sinks for the liquid film are mainly due to the phase change as well as the droplet deposition and entrainment, as shown in Fig. 3.

The phase change model considers evaporation of the liquid film, where some or all of the evaporating liquid is transferred into the gas core. This term is closely related to the energy equation and will be described in the section dealing with the energy transport phenomena.

The droplet deposition is the direct mass source from the dispersed droplets. It is formulated as the deposition rate.

The film entrainment is mainly due to the disturbance waves, and the mechanisms has been experimentally and theoretically investigated, with close relation with the liquid film-gas interfacial shear stress, boiling effect in the liquid film, and the surface tension (Ishii and Grolmes, 1975; Okawa et al., 2003). Modeling of

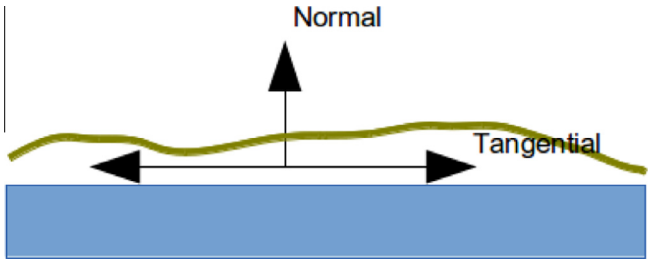

Fig. 2. Schematic of the thin film model and assumed main directions.

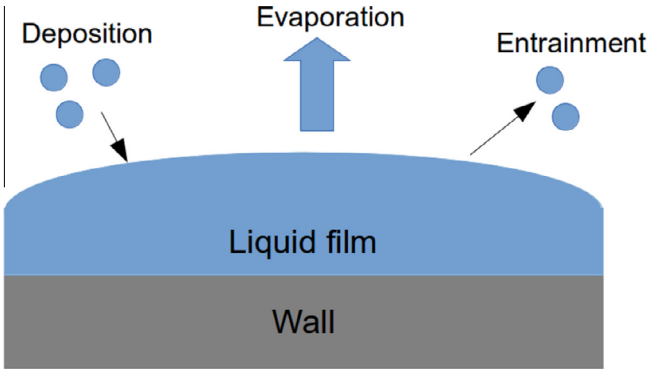

Fig. 3. Schematic of the mass source terms.

the entrainment rates will be discussed in the following section. A certain amount of liquid film will be transferred to the gas core as droplets. Once the properties of entrained droplets are known, e.g. the mass transfer rate and the droplet size, the formulation of the entrainment source term is similar to that of deposition.

When the droplets impinge the liquid film or the wall, they may undergo different behaviors, e.g. stick, spread, rebound and splash (Stanton and Rutland, 1998). For the overall effect, they can all be considered as droplet deposition and entrainment, and can be modeled with different restitution coefficients.

Other mass sources can also be included according to the specific phenomena, e.g. the curvature separation when the liquid film flows around a corner and the dripping when the film flows on the underside of inclined surfaces.

2.1.2. Momentum source terms

As shown in the integrated momentum equation, the source terms for the film momentum have been split into pressure-based part from the tangential gradients in wall normal forces and the stress-based part from the forces in the wall tangential direction.

The pressure-based momentum sources include the local gas phase pressure, the hydrostatic pressure, the capillary pressure, the vapor recoil pressure, and the pressure due to deposition and entrainment, as shown in Fig. 4.

The local gas phase pressure is the gas pressure on the gas–liquid film interface, and can be directly taken from the gas phase results.

The hydrostatic pressure is given by

$$p_\delta = -\rho\delta\mathbf{n}\cdot\mathbf{g} \tag{5}$$

where $\mathbf{n}$ is the surface normal vector, and $\mathbf{g}$ is the gravity vector.

The capillary pressure is due to the surface tension from the liquid film curvature. The term is estimated based on the Laplacian of the liquid film thickness as

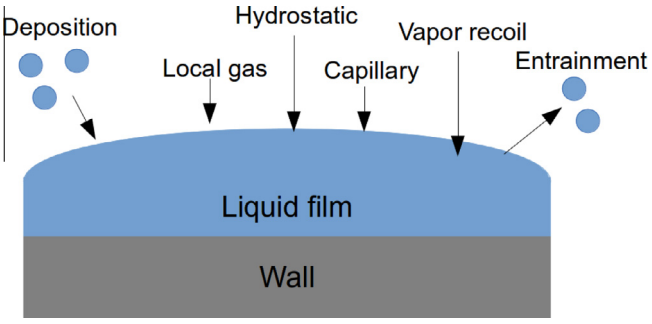

Fig. 4. Schematic of the pressure-based momentum source terms.

$$p_\sigma = -\sigma\nabla_s^2\delta \tag{6}$$

where σ is the surface tension, and $\nabla_s^2\delta$ is the approximation of the local curvature of the liquid film. The approximation is valid only for surfaces with slight curvature.

The vapor recoil pressure is from the vaporization of the liquid film, and can be significant for high evaporation rates. This term is calculated as

$$p_{vap} = \frac{\rho_v u_{vap}^2}{2} = \frac{\dot{m}_{vap}^2}{2\rho_v} \tag{7}$$

where u_{vap} is the surface-normal velocity of the vapor generated at the film surface and $\dot{m}_{vap}$ is the evaporation rate of the liquid film.

Pressure resulting from the droplet deposition is given by

$$p_{dep} = \dot{m}_{dep}(\mathbf{v}\cdot\mathbf{n}) \tag{8}$$

where $\dot{m}_{dep}$ is the droplet deposition rate and $\mathbf{v}$ is the deposited droplet velocity.

In a similar way, the pressure resulting from droplet entrainment can be taken into account.

The stress-based momentum sources consist of gravity force, shear stress, thermocapillary force, contact angle force, and the forces due to droplet deposition and entrainment, as depicted in Fig. 5.

The wall-parallel component of the liquid film acceleration due to gravity force can be taken into account as

$$S_{\mathbf{U},\delta} = \rho\delta\mathbf{g}_t \tag{9}$$

where $\mathbf{g}_t$ is the wall-tangential gravity acceleration.

Based on the thin film assumptions, the velocity profile in the wall normal direction can be simplified as that in the laminar flow. If the wall velocity is zero, the liquid velocity can be defined as

$$\mathbf{u}(z) = \frac{3\overline{\mathbf{U}}}{\delta}\left(z - \frac{1}{2\delta}z^2\right) \tag{10}$$

where $\overline{\mathbf{U}}$ is the mean velocity.

Using this velocity profile, the wall shear stress can be obtained as

$$S_{\mathbf{U},\tau_w} = -\mu_l\left(\frac{\partial\mathbf{u}}{\partial z}\right)\Big|_{z=0} = -\mu_l\frac{3\overline{\mathbf{U}}}{\delta} \tag{11}$$

where μ_l is the viscosity of the liquid film.

The liquid film–gas interface velocity is the boundary for both the liquid film and the gas core flow. To account for the wavy and rough interfacial effect, the interfacial shear stress is evaluated as

$$S_{\mathbf{U},\tau_g} = \frac{C_{f,i}\rho_g|\mathbf{u}_g - \mathbf{u}_f|(\mathbf{u}_g - \mathbf{u}_f)}{2} \tag{12}$$

where $C_{f,i}$ is the friction factor, defined by Wallis (1969) as

$$C_{f,i} = 0.005\left(1 + 300\frac{\delta}{D_h}\right) \tag{13}$$

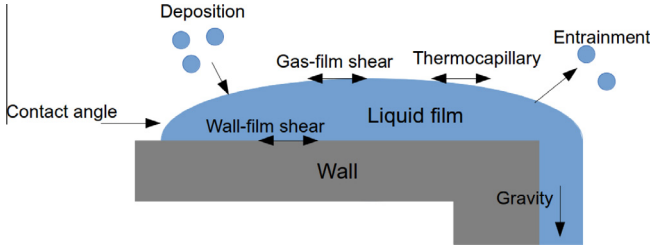

Fig. 5. Schematic of the stress-based momentum source terms.

where D_h is the hydraulic diameter.

The thermocapillary force is due to the Marangoni effect, which is caused by the temperature dependent surface tension variation. The thermocapillary force will drive the fluid from low surface tension regions to the high surface tension regions, which usually means that liquid will move from hot regions to cold regions. It is defined as

$$S_{\mathbf{U},mag} = -\nabla_s \sigma \tag{14}$$

If the wall surface is partially wetted, the surface tension effect will lend a contact angle force on the contact line between the dry and wet regions. The surface tangential force normal to the contact line per unit width of contact line can be expressed as

$$F_c = \sigma(1 - \cos\theta_\sigma) \tag{15}$$

where θ_σ is the contact angle. It should be noted that a critical film thickness is specified as a criterion for dry or wet region according to the wall surface characteristics, e.g. hydrophobic or hydrophilic.

The stress sources from droplet deposition is expressed as

$$S_{\mathbf{U},dep} = \dot{m}_{dep}\mathbf{v}_t \tag{16}$$

where $\mathbf{v}_t$ is the droplet tangential velocity.

The stress sources due to the droplet entrainment rates can be defined in a similar way.

2.1.3. Energy source terms

As shown in Fig. 6, the energy sources include mainly such effects as wall heat transfer, interfacial heat transfer, evaporation, sources from droplet deposition and entrainment, and possibly radiation.

Energy sources resulting from wall heat transfer can be defined according to the boundary conditions at the wall. If the wall temperature is given as the Dirichlet boundary condition, the source term can be simplified assuming the linear temperature profile in the liquid film and it can be expressed as

$$S_{h,q_w} = -k_l\left(\frac{\partial T}{\partial z}\right)\Big|_{z=0} = -k_l\frac{T - T_w}{\delta/2} \tag{17}$$

where k_l is the heat conductivity of the liquid film, T is the mean temperature of the liquid film, and T_w is the wall temperature.

Alternatively, if the wall heat flux is known as the Neumann boundary condition, the source term can be added directly.

Interfacial heat transfer can be similarly defined as

$$S_{h,q_g} = -k_{g,eff}\left(\frac{\partial T}{\partial z}\right)\Big|_{z=\delta} \tag{18}$$

where $k_{g,eff}$ is the effective heat conductivity in laminar or turbulent gas core flow.

The source due to evaporation of the liquid film is defined as

$$S_{h,vap} = S_{\delta,vap}h_{fg} \tag{19}$$

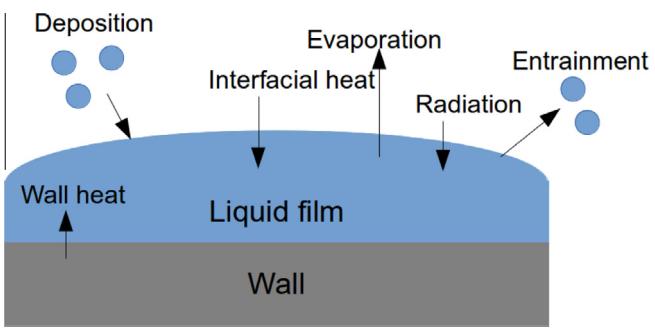

Fig. 6. Schematic of the energy source terms.

where $S_{\delta,vap}$ is the evaporation rate, present as the mass source in the mass equation, and h_{fg} is the latent heat of evaporation.

The evaporation rate can be calculated based on the energy balance for saturated liquid film as

$$S_{\delta,vap} = -\frac{q_{sp}}{h_{fg}} \tag{20}$$

where q_{sp} is the heat flux to the liquid film.

Energy sources resulting from the droplet deposition is expressed as

$$S_{h,dep} = \dot{m}_{dep}h_{dep} \tag{21}$$

where h_{dep} is the droplet enthalpy.

The energy sources from droplet entrainment can be similarly obtained.

In addition, other source terms can be included, e.g. radiation, if the effects are significant for the phenomena under consideration.

2.2. Modeling of gas core flow

In a unified frame for annular flow, the liquid film modeling should be coupled to simultaneous calculation of the gas core flow including gas and dispersed liquid droplets. The gas core flow can be described using the Eulerian–Eulerian or the Eulerian–Lagrangian methods, both of which have been proven to be capable to capture the governing phenomena. In the current work, the Eulerian–Lagrangian technique is employed, partly due to the straightforward formulation of the interaction with the liquid film.

In the Eulerian–Lagrangian framework, the gas phase is treated as a continuum by solving the Reynolds-Averaged Navier–Stokes equations, while the droplets are solved by Lagrangian Particle Tracking (LPT). The droplets can exchange mass, momentum and energy with the gas phase, in consideration of which a two-way coupling method is employed. In two-way coupling, the influence of the droplets to the gas phase is also considered, due to the mutual interaction. However, the interaction between the droplets such as the collision and coalescence is not taken into account, since the modeling of that is still not well established due to the complexity of the involved phenomena.

For turbulence in the gas phase, as mentioned by Damsohn (2011), the wall treatment can be conducted with a high Reynolds number approach, to save computational cost, since the influence of the liquid film at the wall is not considered and the wall cells cannot be considered very accurately. Therefore, a low Reynolds number approach at the wall, and also a spatially-resolved method, e.g. Large Eddy Simulation (LES), are unnecessary. For simplicity, the robust k-omega SST model for the turbulence is employed.

In particle tracking, when the density of the particle is much greater than that of the fluid, the only significant contributions are from the viscous drag, and possibly, the Saffman lift force (Young and Leeming, 1997). Wang et al. (1997) argued that the lift force optimized for shear wall bounded flow is substantially smaller than that obtained using the Saffman lift formula, and furthermore, the overall effect of the lift force is small. As a result, the droplet tracking through the gas flow is solved using the standard Lagrangian equation, where the drag and gravity effects are included, sometimes also with the Saffman lift force included for comparison. The turbulent dispersion of droplets is calculated using the Discrete Random Walking (DRW) method based on the model proposed by Gosman and Ioannides (1983). Although the characteristics of the eddies are for an isotropic flow and it does not well reflect the situation close to the wall, it is sufficiently valid for high-inertia droplets. The droplets obtain enough energy from the bulk flow to arrive at the wall without sensing the flow characteristics close to the wall (Caraghiaur and Anglart, 2013).

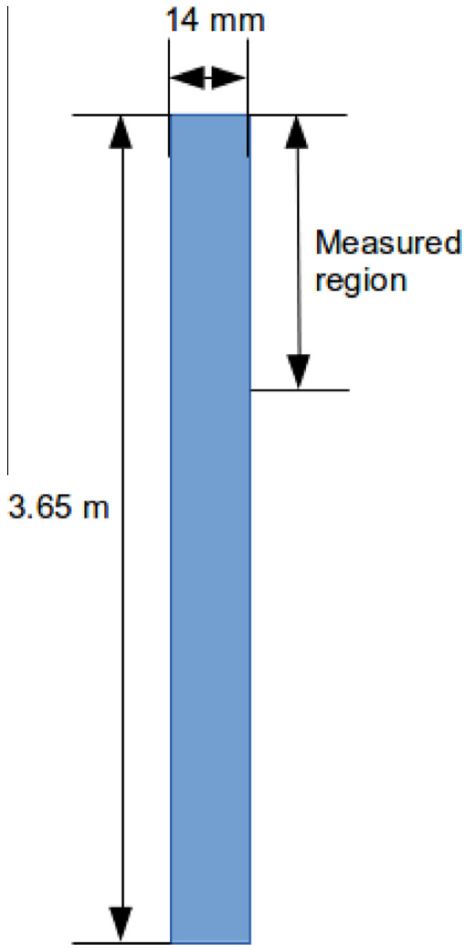

Fig. 7. The test section and the measured region (Adamsson and Anglart, 2006).

2.3. Coupling of the gas core flow with the liquid film

The major interaction of the gas core flow and the liquid film in the annular two phase flow is the evaporation, droplet deposition and entrainment. This means that the three fields of gas, droplets, and liquid film have interfacial transfers of mass, momentum and energy.

In particular, if we consider the mass transfer mechanism, the following terms have to be taken into account. For the gas field, there is mass source due to evaporation of the liquid film, whereas for the liquid film, there is mass source due to the droplet deposition, and finally for the droplets, there is mass source due to entrainment of the liquid film.

In the current model framework, the gas core flow is represented using the Eulerian–Lagrangian method, and therefore the droplets are tracked directly. This makes the coupling of the gas core flow with the liquid film model more straightforward, since the droplet deposition and entrainment can be handled directly. For example, when the droplets are deposited to the wall, the mass can be collected and added to the source term of the mass equation for the liquid film.

3. Model validation

3.1. Test cases

Experiments were carried out in high pressure two-phase flow loop by Adamsson and Anglart (2006), to investigate the influence of the axial power distribution on the liquid film flow and dryout power. It is also the purpose of the current work to model the liquid film, to obtain the liquid film thickness or flow rate, and finally to predict the dryout occurrence, based on criteria of the critical film thickness or the minimum film flow rate (Anglart, 2011).

The measurements were performed under conditions typical for a BWR, with pressure of 7 MPa and total mass flux ranging from 750 to 1750 kg/m^{2}s. As shown in Fig. 7, the test section is a circular vertical pipe with inner diameter of 14 mm and heated length of 3.65 m. All the experiments were carried out at 10 K inlet subcooling, which is at the bottom of the test section. The water flows upward and is heated from subcooled single phase to bubbly, slug, churn, and finally annular flow. The measurements were conducted only in the annular flow region, which is also the calculation region in the current work.

Initially the three cases with uniform wall heat flux distribution are calculated, with measurements of the film flow rate at various

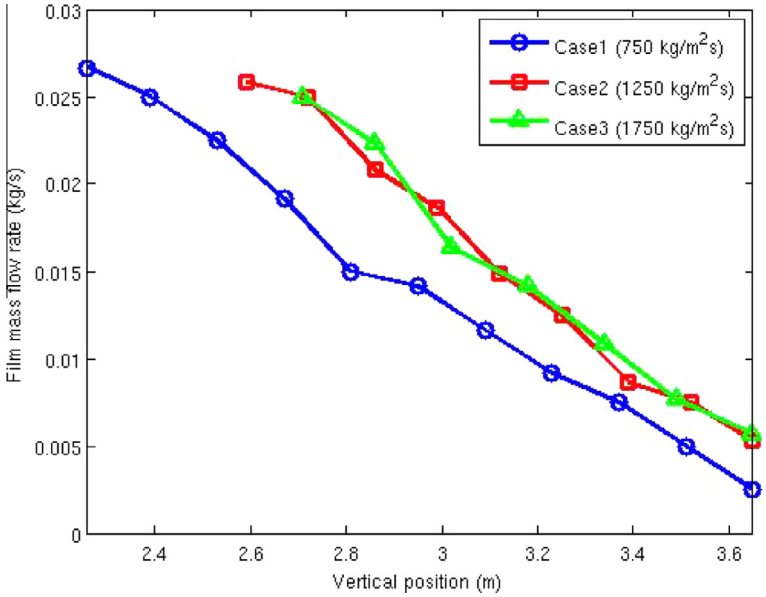

Fig. 8. Measurement of the liquid film flow rate (Adamsson and Anglart, 2006).

Table 1
General data on test cases.

	Case 1	Case 2	Case 3
Inlet mass flux (kg/m^2 s)	750	1250	1750
Measured length (m)	1.39	1.06	0.94

vertical positions as shown in Fig. 8. From the experimental results, the wall heat flux and the corresponding mass flow rate for gas phase and droplets can be evaluated based on energy balance, as shown in Table 1.

3.2. Case setup

In the experiments performed by Adamsson and Anglart (2006), the liquid film flow rate was measured, since the film thickness could not be obtained directly. Therefore, the inlet film thickness, which is needed in the present calculations, is evaluated to be 0.4, 0.3, and 0.25 mm for cases 1, 2, and 3 based on the correlations (Adamsson and Le Corre, 2011), and then the inlet velocity is calculated based on the measured film flow rate.

For the gas phase, the inlet flow rate is specified, and the outlet pressure is fixed at 7 MPa.

The droplets are injected from the inlet of the measured region with uniformly distributed random initial positions, and the initial velocities are specified the same as those of the gas phase. The droplet size was not measured, and for simplicity, it is estimated using correlations developed by Caraghiaur and Anglart (2013). The estimated droplet size was stated to be with ±40% of uncertainty (Caraghiaur and Anglart, 2013). The sensitivity study in the current work has shown that the resultant liquid film thickness

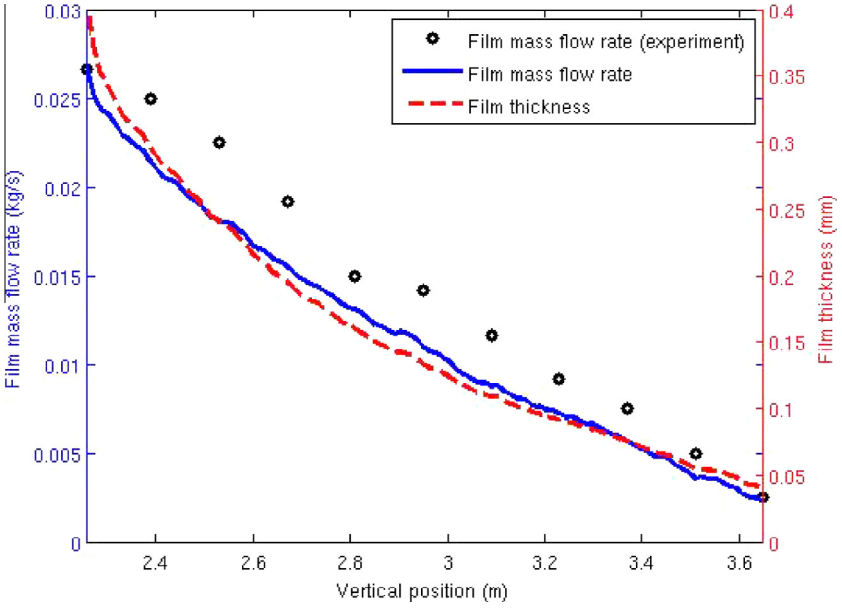

Fig. 9. Liquid film flow rate and thickness for case 1.

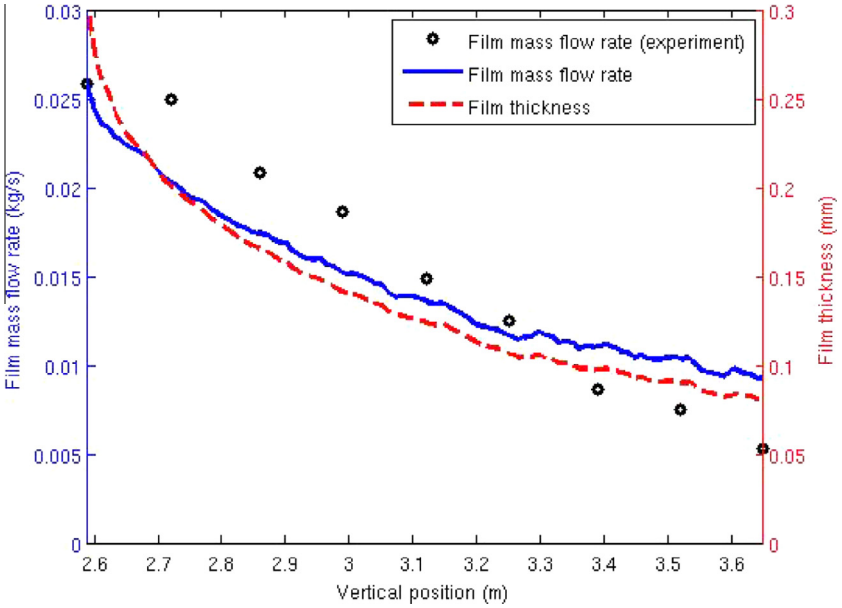

Fig. 10. Liquid film flow rate and thickness for case 2.

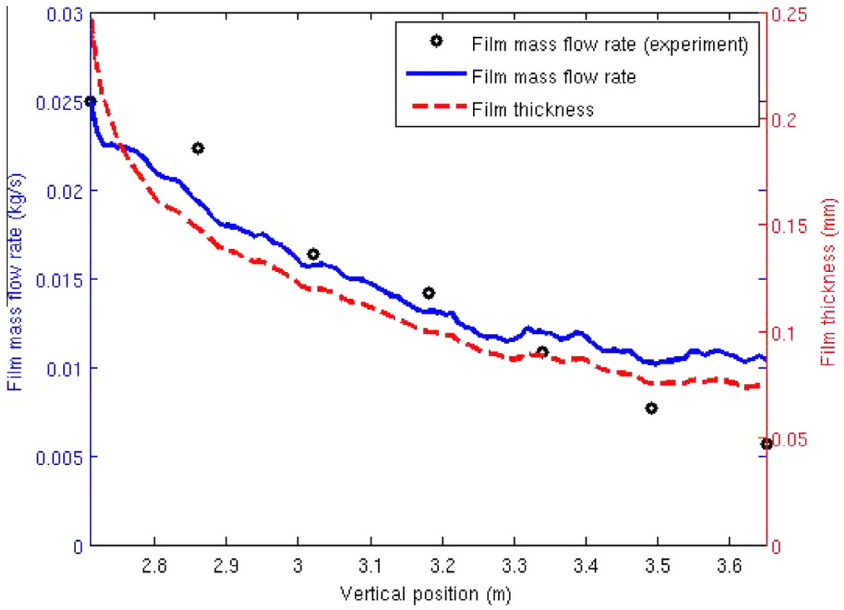

Fig. 11. Liquid film flow rate and thickness for case 3.

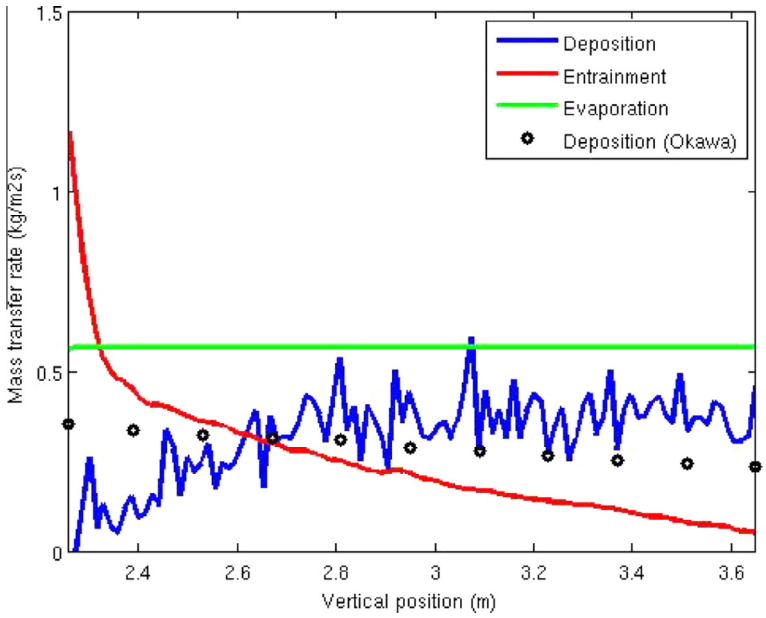

Fig. 12. Interactive mass transfer rates for case 1.

and flow rate is not significantly influenced within the ±40% uncertainty. Therefore, the fixed droplet size has been used for each of the three cases, which correspond to 0.06 (case 1), 0.053 (case 2), and 0.048 mm (case 3).

When the droplets arrive at the wall, they will interact with the liquid film. In the current work, the full absorptions of the droplets are considered as a reasonable assumption. Once the droplets are absorbed by the liquid film, they will not be tracked, and instead they will be included in the liquid film as a mass source as described in previous sections. When the droplets hit the outlet (or inlet) boundaries, they will be removed from the computational domain.

As stated previously, the disturbance-waves-induced entrainment should be included as a source term of the mass transfer. Usually the droplet entrainment was modeled based on experiment-based correlations, instead of fully resolving the wavy thin liquid film, which is too expensive for practical applications. The existing developed correlations, however, were based on the channel-averaged one-dimensional flow conditions. In current work, the gas core flow conditions used in the correlations were taken from the film-adjacent cells. The advantage of this approach is that the entrainment rate is formulated based on the local flow conditions. Needless to say, however, that more validations of the approach will be needed in the future work. Correlations for entrainment rate and entrainment fraction have then been proposed based on experimental results and theoretical analysis (Hewitt and Govan, 1990; Kataoka et al., 2000; Okawa and Kataoka, 2005; Sawant et al., 2009). Assuming that the entrain-

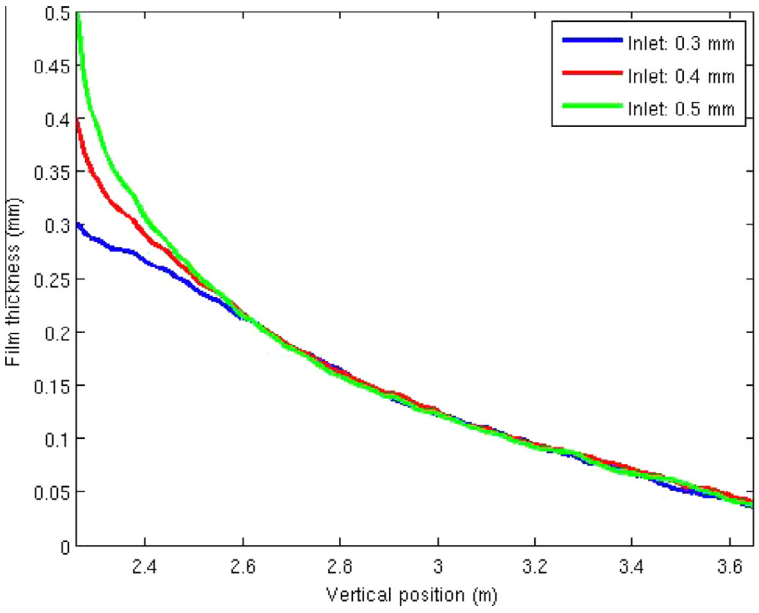

Fig. 13. Solution sensitivity to the inlet film thickness.

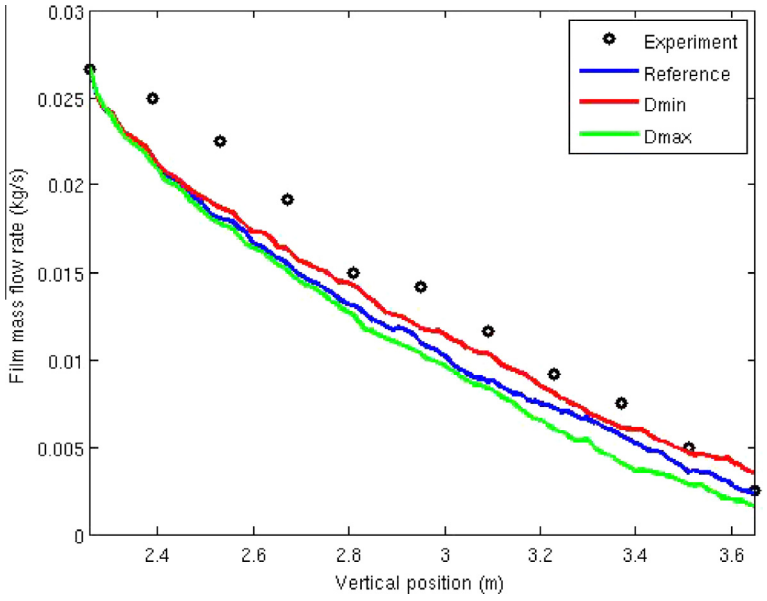

Fig. 14. Solution sensitivity to the droplet size.

ment rate is proportional to the interfacial shear force and inversely proportional to the surface tension force, the entrainment rate is developed by Okawa et al. (2003) as

$$S_{\delta,ent} = -k_e \rho_l \frac{C_{f,i} \rho_g J_g^2 \delta}{\sigma} \left(\frac{\rho_l}{\rho_g} \right)^{0.111} \tag{22}$$

where J_g is the gas volumetric flux, k_e is a coefficient given by

$$k_e = -4.79 \times 10^{-4} \text{ m/s} \tag{23}$$

and $C_{f,i}$ is the friction factor defined in Eq. (13).

From available experimental data, disturbance waves are not formed when the liquid film Reynolds number is below the critical value. For this reason, the criterion for the inception of entrainment is

$$\text{Re}_f > 320 \tag{24}$$

where Re_f is the liquid film Reynolds number and is defined as

$$\text{Re}_f = \frac{\rho_l J_f D_h}{\mu_l} \tag{25}$$

where J_f is the liquid film volumetric flux. If the inception criterion is not satisfied, the droplet entrainment is not present.

When the liquid film is entrained into the gas core flow as droplets, the initial sizes of the droplets are assumed to be the same as those of the inlet droplets. The initial position is put in the surface of the liquid film and the initial velocity is defined the same as that of the local liquid film. Clearly, the entrained droplets can be redeposited to the liquid film, if they get sufficient momentum from the gas core flow.

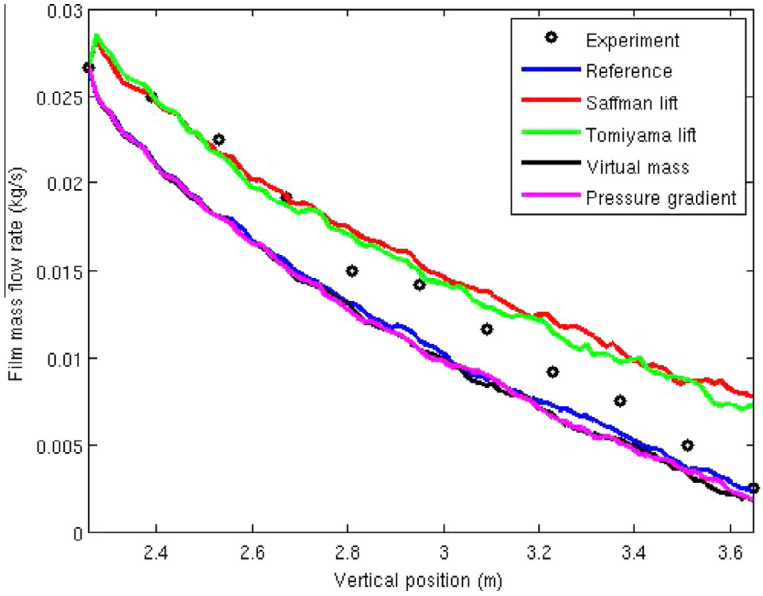

Fig. 15. Solution sensitivity to various forces acting on droplets.

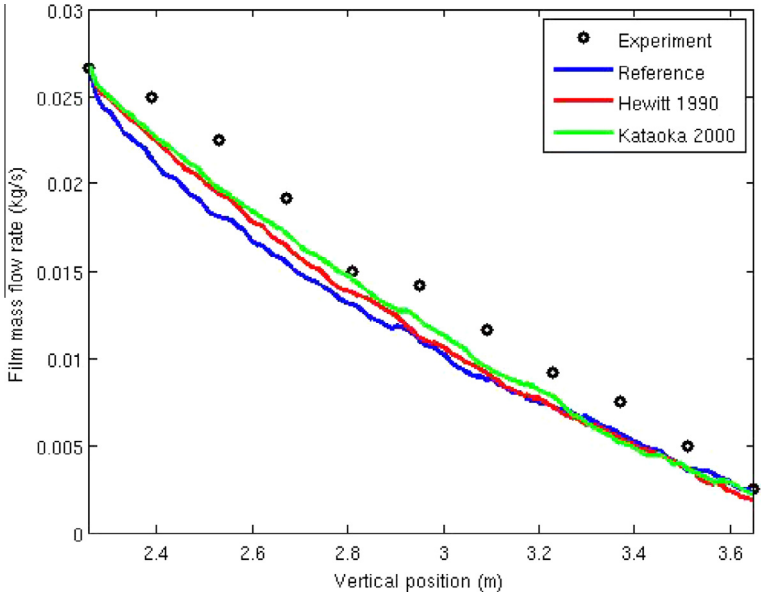

Fig. 16. Solution sensitivity to various entrainment correlations.

3.3. Results and discussion

The simulation results for the three cases have been shown in Figs. 9–11. Since the liquid film thickness was not measured in the experiments, only the liquid film flow rate is compared to the measurements. Generally the calculated liquid film flow rate agrees quite well with the measurements. The results for all three cases show that the liquid film flow rate was under-predicted at the entrance region of the pipe length. This could be explained by the decreased entrainment rate along the pipe, with gradually depleted liquid film thickness. On the other hand, as the gas core flow develops along the pipe, the gas velocity near the pipe wall will decrease from the assumed uniform velocity distribution at the inlet. This will induce more deposition, since the droplets respond more readily to the turbulence, which accounts for the over-prediction of the liquid film flow rate in the second half of the pipe length. Other possible explanations could also be expected such as the effects due to the droplet interaction, e.g. the coalescence of the droplets, which is not included here and may be considered as the future work.

To better illustrate the results, the mass transfer rate of liquid film evaporation, droplet deposition and entrainment are also shown in Fig. 12, with comparisons to the deposition rate evaluated based on experimental data using correlations from Okawa et al. (2003). The deposition rate results show good agreement with the correlation, and deviations near the inlet could be due to the inlet droplet particle injection models.

3.4. Sensitivity analysis

Some of the input parameters and boundary conditions for current test cases were determined based on estimations, which may

significantly influence the final calculation results. For that reason, sensitivity analysis was carried out to identify the key parameters for further studies. The sensitivity for inlet film thickness, droplet size, droplet forces, and entrainment correlations were included in the current work. For clarity, all the sensitivity results were based on case 1.

As mentioned before, the inlet film thickness was estimated as 0.4 mm for case 1 based on the correlations (Adamsson and Le Corre, 2011). The inlet velocity then is determined, since the inlet liquid film flow rate can be obtained from the measurements. Fig. 13 shows the liquid film thickness results with regard to different inlet values of the thickness. Since the film flow rate is the same, this inlet effect will disappear in a short distance. This means that the assumed inlet film thickness is not influential if the film flow rate is kept the same.

The droplet size was assumed to be fixed and is estimated as 0.06 mm for case 1 using correlations developed by Caraghiaur and Anglart (2013). The estimated droplet size was stated to be with ±40% of uncertainty (Caraghiaur and Anglart, 2013). As a result, Fig. 14 shows the film flow rate results for different droplet sizes ranging from −40% to 40% of the reference value. With larger droplets, the film flow rate is lower than the reference one. This is mainly due to the reduction in deposition rate with increasing particle size, which is explained by the fact that the increasing particle inertia results in a decreasing response to the turbulence.

Fig. 15 shows the film flow rate results for different droplet forces. In the reference case, only the drag and gravity were included as the droplet-gas interaction forces. The Saffman lift force, Tomiyama lift force, virtual mass force, and pressure gradient force were separately added to the drag and gravity forces. It shows that film flow rate for cases with lift force, either Saffman lift or Tomiyama lift, over-predict the deposition, as described by Wang et al. (1997). Furthermore, the effects from the virtual mass force and pressure gradient force are negligible.

The entrainment was calculated based on correlations in the current work. Correlations from Okawa et al. (2003), Hewitt and Govan (1990), and Kataoka et al. (2000) were tested here as shown in Fig. 16. It shows that the Reference Okawa et al. (2003) correlation predicts a higher entrainment rate.

4. Summary and conclusions

With the objective to predict the dryout occurrence based on the criteria of the liquid film thickness, a computational fluid dynamics (CFD) model of annular two-phase flow with evaporating liquid film has been developed based on the two-dimensional modeling of liquid film. The liquid film flow model is integrated in the wall normal direction, based on the thin-film assumption that the flow in the wall normal direction can be neglected, and the spatial gradients of the dependent variables tangential to the wall are negligible compared to those in the wall normal direction. The liquid film model has been coupled to the gas core flow, using an Eulerian–Lagrangian technique to obtain a unified framework for annular flow. The mass, momentum and energy transfer between the liquid film, gas, and entrained droplets has been taken into account.

The resultant unified model for annular flow has been applied to the steam–water flow with conditions typical for a BWR. The liquid film flow rate generally decreases with the combined effects of evaporation, and droplets deposition and entrainment. The simulation results for the liquid film flow rate show favorable agreement with the experimental data, with the potential to predict the dryout occurrence based on the criteria of the critical film thickness or the critical film flow rate.

Acknowledgement

The present work is partially funded by the European Commission under the 7th EUROATOM Framework Program within the NURESAFE Project contract No. 323263.

References

Adamsson, C., Anglart, H., 2006. Film flow measurements for high-pressure diabatic annular flow in tubes with various axial power distributions. Nucl. Eng. Des. 236, 2485–2493.
Adamsson, C., Le Corre, J., 2011. Modeling and validation of a mechanistic tool (MEFISTO) for the prediction of critical power in BWR fuel assemblies. Nucl. Eng. Des. 241, 2843–2858.
Adechy, D., Issa, R.I., 2004. Modelling of annular flow through pipes and T-junctions. Comput. Fluids 33, 289–313.
Anglart, H., 2011. Onset of stable dryout condition in diabatic annular two-phase flow. In: The 14th International Topical Meeting on Nuclear Reactor Thermal-Hydraulics, NURETH-14, p. 226.
Anglart, H., 2013. Investigation of local dryout conditions in forced convection to water at high pressure in uniformly and non-uniformly heated vertical round tubes and annuli. In: The 15th International Topical Meeting on Nuclear Reactor Thermal-Hydraulics, NURETH-15, p. 117.
Bai, C., Gosman, A.D., 1996. Mathematical Modelling of Wall Films Formed by Impinging Sprays. SAE Technical Paper 960626.
Caraghiaur, D., Anglart, H., 2013. Drop deposition in annular two-phase flow calculated with Lagrangian Particle Tracking. Nucl. Eng. Des. 265, 856–866.
Damsohn, M., 2011. Liquid Films and Droplet Deposition in a BWR Fuel Element (PhD Thesis). ETH, Zurich.
Gosman, A.D., Ioannides, E., 1983. Aspects of computer simulation of liquid-fueled combustors. J. Energy 7 (6), 482–490.
Hewitt, G.F., Govan, A.H., 1990. Phenomenological modelling of non-equilibrium flows with phase change. Int. J. Heat Mass Transf. 33 (2), 229–242.
Ishii, M., Grolmes, M.A., 1975. Inception criteria for droplet entrainment in two-phase concurrent film flow. AIChE J. 21 (2), 308–318.
Kataoka, I., Ishii, M., Nakayama, A., 2000. Entrainment and deposition rates of droplets in annular two-phase flow. Int. J. Heat Mass Transf. 43, 1573–1589.
Lahey Jr., R.T., 2005. The simulation of multidimensional multiphase flows. Nucl. Eng. Des. 235, 1043–1060.
Meredith, K., Xin, Y., De Vries, J., 2011. A numerical model for simulation of thin-film water transport over solid fuel surfaces. In: Fire Safety Science – Proceedings of the Tenth International Symposium, pp. 415–428.
Okawa, T., Kataoka, I., 2005. Correlations for the mass transfer rate of droplets in vertical upward annular flow. Int. J. Heat Mass Transf. 48, 4766–4778.
Okawa, T., Kotani, A., Kataoka, I., Naito, M., 2003. Prediction of critical heat flux in annular flow using a film flow model. J. Nucl. Sci. Technol. 40 (6), 388–396.
Rodriguez, J.M., 2009. Numerical Simulation of Two-phase Annular Flow (PhD Thesis). Rensselaer Polytechnic Institute, New York, USA.
Sawant, P., Ishii, M., Mori, M., 2009. Prediction of amount of entrained droplets in vertical annular two-phase flow. Int. J. Heat Fluid Flow 30, 715–728.
Stanton, D.W., Rutland, C.J., 1998. Multi-dimensional modeling of thin liquid films and spray-wall interactions resulting from impinging sprays. Int. J. Heat Mass Transf. 41, 3037–3054.
Tong, L.S., Tang, Y.S., 1997. Boiling Heat Transfer and Two-phase Flow. Taylor and Francis, Washington, D.C., USA.
Wallis, G.B., 1969. One-dimensional Two-phase Flow. McGraw-Hill, New York, USA.
Wang, Q., Squires, K.D., Chen, M., McLaughlin, J.B., 1997. On the role of the lift force in turbulence simulations of particle deposition. Int. J. Multiphase Flow 23 (4), 749–763.
Yamamoto, Y., Okawa, T., 2010. Numerical study of particle concentration effect on deposition characteristics in turbulent pipe flows. J. Nucl. Sci. Technol. 47 (10), 945–952.
Young, J., Leeming, A., 1997. A theory of particle deposition in turbulent pipe flow. J. Fluid Mech. 340, 129–159.
Zuber, N., Staub, F.W., 1966. Stability of dry patches forming in liquid films flowing over heated surfaces. Int. J. Heat Mass Transf. 9, 897–905.